Cellulose Structural Polymorphism in Plant Primary Cell Walls Investigated by High-Field 2D Solid-State NMR Spectroscopy and Density Functional Theory Calculations

Citation: Wang, Tuo et al. "Cellulose Structural Polymorphism in Plant Primary Cell Walls Investigated by High-Field 2D Solid-State NMR Spectroscopy and Density Functional Theory Calculations." Biomacromolecules 17, 6 (May 2016): 2210–2222 © 2016 American Chemical Society

As Published: http://dx.doi.org/10.1021/ACS.BIOMAC.6B00441

Publisher: American Chemical Society (ACS)

Persistent URL: http://hdl.handle.net/1721.1/113319

Version: Author's final manuscript: final author's manuscript post peer review, without publisher's formatting or copy editing

HHS Public Access

Author manuscript

Biomacromolecules. Author manuscript; available in PMC 2017 January 27.

Published in final edited form as:

Biomacromolecules. 2016 June 13; 17(6): 2210–2222. doi:10.1021/acs.biomac.6b00441.

Cellulose Structural Polymorphism in Plant Primary Cell Walls Investigated by High-Field 2D Solid-State NMR Spectroscopy and Density Functional Theory Calculations

Tuo Wang[1], **Hui Yang**[2], **James D. Kubicki**[3], and **Mei Hong**[1,*]

[1]Department of Chemistry, Massachusetts Institute of Technology, Cambridge, MA 02139

[2]Department of Geosciences, The Pennsylvania State University, University Park, PA 16802

[3]Department of Geological Sciences, University of Texas at El Paso, El Paso, TX 79968

Abstract

The native cellulose of bacterial, algal, and animal origins has been well studied structurally using X-ray and neutron diffraction and solid-state NMR spectroscopy, and is known to consist of varying proportions of two allomorphs, Iα and Iβ, which differ in hydrogen bonding, chain packing, and local conformation. In comparison, cellulose structure in plant primary cell walls is much less understood because plant cellulose has lower crystallinity and extensive interactions with matrix polysaccharides. Here we have combined two-dimensional magic-angle-spinning (MAS) solid-state nuclear magnetic resonance (solid-state NMR) spectroscopy at high magnetic fields with density functional theory (DFT) calculations to obtain detailed information about the structural polymorphism and spatial distributions of plant primary-wall cellulose. 2D ^{13}C-^{13}C correlation spectra of uniformly ^{13}C-labeled cell walls of several model plants resolved seven sets of cellulose chemical shifts. Among these, five sets (denoted *a*-*e*) belong to cellulose in the interior of the microfibril while two sets (*f* and *g*) can be assigned to surface cellulose. Importantly, most of the interior cellulose ^{13}C chemical shifts differ significantly from the ^{13}C chemical shifts of the Iα and Iβ allomorphs, indicating that plant primary-wall cellulose has different conformations, packing and hydrogen bonding from celluloses of other organisms. 2D ^{13}C-^{13}C correlation experiments with long mixing times and with water polarization transfer revealed the spatial distributions and matrix-polysaccharide interactions of these cellulose structures. Cellulose *f* and *g* are well mixed chains on the microfibril surface, cellulose *a* and *b* are interior chains that are in molecular contact with the surface chains, while cellulose *c* resides in the core of the microfibril, outside spin diffusion contact with the surface. Interestingly, cellulose *d*, whose chemical shifts differ most significantly from those of bacterial, algal and animal cellulose, interacts with hemicellulose, is poorly hydrated, and is targeted by the protein expansin during wall loosening. To obtain information about the C6 hydroxymethyl conformation of these plant celluloses, we

[*]**Corresponding Author**: meihong@mit.edu.

Supporting Information

The structural parameters of glucose units in DFT calculation are shown in Table S1. The estimated fractions of glucose conformers in Iα and Iβ allomorphs are shown in Table S2. The ^{13}C RMSDs between measured and calculated ^{13}C chemical shifts are shown in Table S3. NMR pulse sequences are shown in Fig. S1. The assignment of *Brachypodium* cellulose signals is shown in Fig. S2. The 2D ^{13}C-^{13}C 30 ms PDSD spectrum of *Arabidopsis* cell walls is shown in Fig. S3. The 2D ^{13}C- ^{13}C long-mixing PDSD spectra of *Brachypodium* samples are shown in Fig. S4, 5. The ^{13}C-T_1 filtered PDSD spectra of *Brachypodium* cell walls are shown in Fig. S6.

carried out DFT calculations of ^{13}C chemical shifts, using the Iα and Iβ crystal structures as templates and varying the C5-C6 torsion angle. Comparison with the experimental chemical shifts suggests that all interior cellulose favor the *tg* conformation, but cellulose *d* also has a similar propensity to adopt the *gt* conformation. These results indicate that cellulose in plant primary cell walls, due to their interactions with matrix polysaccharides, has polymorphic structures that are not a simple superposition of the Iα and Iβ allomorphs, thus distinguishing them from bacterial and animal celluloses.

Introduction

Cellulose is a linear chain of β(1–>4)-D-glucose units that hydrogen-bonds side by side in a parallel fashion to form microfibrils of varying thicknesses. Cellulose is produced by many organisms, including bacteria, algae, plants and some marine animals [1], but its largest source is plant cell walls, which are estimated to produce 120–140 billion tons of cellulose globally every year [2]. ^{13}C magic-angle-spinning (MAS) solid-state NMR (solid-state NMR) spectroscopy has been applied since the 1980's to understand the principal structural features of native cellulose [3–5]. Based on ^{13}C NMR chemical shifts, cellulose from many sources was found to consist of two crystalline allomorphs, Iα and Iβ, in varying proportions [4]. Cellulose of bacteria and algae such as *Acetobacter xylinum* and *Valonia* is dominated by the Iα allomorph, while cellulose of the secondary cell walls of higher plants such as cotton and ramie mainly contains the Iβ allomorph. These two allomorphs are distinguished by their C1, C4 and C6 chemical shifts: referenced to tetramethylsilane (TMS), the Iα allomorph exhibits a C1 chemical shift of 105 ppm and a C4 doublet at 90 ppm and 89 ppm, while the Iβ allomorph exhibits a C1 doublet at 106 ppm and 104 ppm and C4 chemical shifts of 89 ppm and 88 ppm. Recently, 2D ^{13}C-^{13}C and ^{13}C-^{1}H correlation NMR experiments were carried out on highly crystalline bacterial (*Acetobacter xylinum*), algal (*Cladophora*), and animal (tunicate) cellulose [6, 7] to definitively assign the chemical shifts of the Iα and Iβ allomorphs. These data resolved two sets of ^{13}C chemical shifts for each allomorph with equimolar intensities, indicating two magnetically inequivalent glucopyranose rings in each allomorph. The A and A' structures in Iα cellulose are spatially close together, as manifested by inter-residue cross peaks in 2D ^{13}C-^{13}C correlation spectra, while the B and B' structures in Iβ cellulose are well separated [8]. These results are in excellent agreement with crystal structures [9, 10], which showed that Iα cellulose contains identical chains with alternating glucose units with slightly different structures, while Iβ cellulose contains two types of chains that are separated in alternating sheets.

Compared to highly crystalline cellulose of bacteria, algae, and animals, plant primary cell wall cellulose is much less understood because of its extensive interactions with matrix polysaccharides, which give rise to low crystallinity and relatively small lateral dimensions (3–5 nm) [11, 12]. These properties make primary-wall cellulose structure challenging to study at the molecular level. High-resolution structural information of primary-wall cellulose is important for understanding the physical and biochemical properties of plant cell walls and the mechanism of wall loosening during plant growth [13]. Recently, we employed ^{13}C isotopic labeling of whole plants and 2D and 3D correlation solid-state NMR techniques to investigate the structure and dynamics of primary-wall polysaccharides under near-native

conditions [14–18]. The multidimensional correlation approach allowed us to resolve and assign the ^{13}C signals of wall polysaccharides and identify long-range cross peaks that are indicative of intermolecular interactions among wall polymers [19, 20]. ^{13}C labeling also facilitated the measurement of quantitative ^{13}C NMR spectra to investigate the size of the cellulose microfibril. The number of glucan chains constituting the plant cellulose microfibrils has been a topic of active debate [13, 21]. The original proposal was that the microfibril contains 36 chains, based on the hexameric organization of the cellulose synthase complex (CSC) in the plasma membrane [22]. However, this number was recently revised to 18–24 based on joint analyses of ^{13}C NMR spectra and X-ray scattering data [23–27], MD simulations [28] and biochemical analysis of the stoichiometry of different isoforms of cellulose synthase [29]. Our recent quantitative ^{13}C solid-state NMR spectra yielded surface-to-interior cellulose intensity ratios that correspond to at least 24 chains for primary-wall microfibrils [19]. This number is consistent with long-mixing-time 2D correlation spectra that show that some interior cellulose chains are deeply embedded in the microfibril and are outside ^{13}C spin diffusion reach of the surface chains. While these NMR data suggest more than 18–24 chains for primary-wall cellulose microfibrils, it remains to be determined whether this larger number reflects the size of isolated microfibrils or partly coalesced microfibrils, as seen, for example, in onion cell walls by AFM [30, 31].

In this work, we have resolved and identified five types of interior cellulose and two types of surface cellulose structures in the primary cell walls of both dicot and monocot plants. We resolved this multitude of cellulose structures from 2D ^{13}C-^{13}C correlation spectra measured at high magnetic fields of 18.8 and 21.1 Tesla, which correspond to ^{1}H Larmor frequencies of 800 and 900 MHz. Interestingly, the ^{13}C chemical shifts of most types of interior cellulose differ by more than 2 ppm from the chemical shifts of bacterial, algal and animal cellulose, indicating that the structures of plant primary-wall cellulose are not only polymorphic but also significantly different from the Iα and Iβ crystalline allomorphs. Using water polarization transfer experiments, long-range intermolecular correlation experiments, and comparison of wild-type and mutant cell walls, we obtained information about the spatial distribution and matrix-polysaccharide interactions of the different types of cellulose. Finally, using DFT calculations, we propose the hydroxymethyl conformation for the primary-wall cellulose.

Materials and Methods

Plant materials

We measured and compared six primary cell wall samples in this study, including two grass cell walls, *Brachypodium* [17] and *Zea Mays*, and four *Arabidopsis* cell walls, including a wild-type (WT) intact cell wall [18], an *xxt1xxT2xxt5* mutant cell wall [14], a cesa1^{aegeus}/cesa3$^{ixr1\text{-}2}$ mutant cell wall [32], and a WT cell wall that has been digested with CDTA, Na_2CO_3, enzymes and 1M NaOH to remove most of the matrix polysaccharides [33]. The *Brachypodium*, *Zea Mays* and wild-type *Arabidopsis* samples were never dried, while the *xxt1xxT2xxt5* and cesa1^{aegeus}/cesa3$^{ixr1\text{-}2}$ mutants were air-dried and then rehydrated to ~40 wt%. Our recent study showed that polysaccharides in dried and rehydrated cell walls have the same molecular structure and dynamics as those in never-dried cell walls[18]. Detailed

sample preparation procedures have been reported previously. Briefly, uniformly ^{13}C-labeled plant materials were obtained by growing seedlings in the dark for 14 days in liquid culture containing ^{13}C-labeled glucose as the sole carbon source. The seedlings were harvested and ground in liquid nitrogen. Starch and intracellular proteins were removed by treatment with α-amylase and pronase. The resulting insoluble cell wall materials were packed into 3.2 mm MAS rotors for solid-state NMR experiments.

Solid-State NMR experiments

1D ^{13}C cross-polarization (CP) MAS spectra were measured on 800 MHz (18.8 Tesla) and 900 MHz (21.1 Tesla) Bruker NMR spectrometers using 3.2 mm MAS probes. Typical radiofrequency (rf) field strengths were 62.5 kHz for ^{13}C and 62.5 - 83 kHz for ^{1}H. All ^{13}C chemical shifts were referenced to the adamantine CH_2 peak at 38.48 ppm on the TMS scale. A 2D radio-frequency-driven recoupling (RFDR) correlation experiment [34] (Fig. S1a) was conducted on the *Brachypodium* cell wall to assign intra-residue cross peaks. The RFDR spectrum was measured under 16 kHz MAS and 83 kHz ^{1}H decoupling. A train of π pulses in the middle of each rotor period recouples the ^{13}C-^{13}C dipolar couplings for longitudinal polarization transfer. A recoupling time of 1.5 ms was used to detect one-bond ^{13}C-^{13}C cross peaks. This mixing time was chosen to selectively detect one-bond cross peaks based on tests on the model peptide formyl-Met-Leu-Phe (MLF) [35, 36]. At this mixing time, one-bond ^{13}C-^{13}C cross peaks have 17–32% of the intensities of diagonal peaks while two-bond cross peaks have less than 2% of the diagonal intensities. 2D proton-driven ^{13}C spin diffusion (PDSD) experiments [37] were conducted on all cell walls using mixing times of 30 ms and 1.0 s, which have been shown previously to give multi-bond intramolecular cross peaks and long-range intermolecular cross peaks (Fig. S1b), respectively [16, 18, 20]. All PDSD spectra were measured at 296 K under 10 kHz MAS. Most 2D spectra were processed using a QSINE window function with an SSB parameter of 2.5–3.0. The number of scans range from 32 to 96 and the signal-to-noise ratios are 10–70 for intermolecular cellulose cross peaks and 30–600 for intramolecular cross peaks. For the RFDR spectrum of the *Brachypodium* cell wall, the lowest contour level was 6% of the highest diagonal peak (75, 75 ppm), the level increment was 1.5, and 24 levels were plotted, so that the highest contour level is 67% of the highest peak. All PDSD spectra were plotted using a minimum contour level of 1% of the highest diagonal peak, which is the (72.5, 72.5 ppm) peak for most cell walls. The highest plotted contour level is ~35% of the highest peak for the 30 ms PDSD spectra and 70–80% of the highest peak for the 1.0 s PDSD spectra.

A ^{1}H T_2 filtered PDSD experiment (Fig. S1c) was conducted on the *Brachypodium* cell wall to detect well-hydrated cellulose. The ^{1}H T_2 filter time was 1.2 ms, which suppressed the polysaccharide ^{1}H magnetization to ~2% while retaining ~55% of the water ^{1}H magnetization. A ^{1}H mixing time (t_{m1}) of 1 ms was used to transfer the water ^{1}H polarization to polysaccharides, and a 30 ms ^{13}C mixing time (t_{m2}) was applied to detect intra-residue polysaccharide cross peaks. The resulting 2D spectra exhibit the signals of hydrated polysaccharides. The experiment was carried out at 263 K under 10 kHz MAS.

A ^{13}C T_1 filtered PDSD experiment was carried out to compare nanosecond-timescale motions of different celluloses. A variable ^{13}C longitudinal mixing period was inserted

before the evolution period of the PDSD experiment (Fig. S1d). Polysaccharides with long ^{13}C T_1 relaxation times retain the signals while polysaccharides with short T_1 relaxation times show weaker signals. The spectra were measured at 296 K under 10 kHz MAS and the ^{13}C spin diffusion mixing time was 30 ms.

DFT calculations

Cellulose Iα and Iβ models with three different conformations of the C6 exocyclic group (*gg*, *gt* and *tg*) were created based on X-ray and neutron diffraction structures [9, 10]. The atomic positions of these models have been previously energy-minimized with periodic DFT-D2 calculations [38, 39]. Clusters consist of four monomer units per chain, three chains wide and four layers high. This allows for four monomers to have at least one other unit next to them in all three dimensions to represent the atomic environment in cellulose. The ends of tetramer chains were terminated with a methyl group to satisfy the bonding of the terminal atoms. The atoms were then held fixed into the positions determined by periodic energy minimizations for calculating isotropic ^{13}C chemical shifts based on the cluster model. Structural parameters such as the inter-atomic distances and torsion angles are listed in Table S1.

NMR shielding tensors were calculated using the modified Perdue-Wang exchange-correlation functional mPW1PW91 [40] and the 6-31G(d) basis set [41] using the Gauge-independent atomic orbitals (GIAO) [42–47] method in Gaussian 09 [48]. Chemical shifts were calculated using the multi-reference method. Methanol was the secondary chemical shift standard, because it produces $\delta^{13}C$ in better agreement with experiments [38, 39, 49, 50]. An empirical correction of 49.5 ppm [51] was used for the difference between the $\delta^{13}C$ of methanol and TMS [49]. This is added to the calculated shielding of methanol to give a corrected isotropic chemical shielding of 193.0 ppm, which is then used to convert the computed cellulose chemical shielding $\sigma^{13}C_i$ for atom i to chemical shift $\delta^{13}C_i$.

$$\delta^{13}C_i = 193.0\text{ppm} - \sigma^{13}C_i$$

Results and Discussion

Structural polymorphism of plant primary wall cellulose

To better resolve the chemical shifts of cellulose in intact plant cell walls, we measured ^{13}C NMR spectra at high magnetic fields corresponding to ^{1}H Larmor frequencies of 800 and 900 MHz. Fig. 1a shows the 1D ^{13}C CP-MAS spectrum of *Arabidopsis* primary cell walls at 900 MHz. Despite the high field, most cellulose signals still overlap with the matrix polysaccharide signals at common C1 chemical shifts of ~105 ppm and at C2, C3, C5 chemical shifts of 70-75 ppm (Fig. 1a). The interior cellulose C4 and C6 peaks (iC4 and iC6) are resolved from matrix polysaccharide signals, but the 2-3 ppm linewidths are still insufficient for resolving multiple structures of cellulose. The fact that multiple structures exist can be seen when window functions that increase the intensities of the middle part of the time-domain signals are applied [23, 52]. With such a window function, the iC4 peak at ~89 ppm reveals three partially resolved peaks while the iC6 peak at ~65 ppm contains at least two peaks. The iC4 fine features resemble a superposition of the Iα allomorph's C4

chemical shifts (90 and 89 ppm) and the Iβ C4 chemical shifts (89 and 88 ppm) [4, 53]. These fine features are present in multiple plants, including *Arabidopsis*, *Brachypodium* and *Zea Mays* (Fig. 1b-e), suggesting that this structural polymorphism is common to plant primary-wall cellulose. Chemical and enzymatic digestion of matrix polysaccharides in the *Arabidopsis* primary walls did not remove these fine features (Fig. 1c), indicating that the cellulose structural polymorphism is robust.

Extending the experiments to two dimensions at high fields resolved multiple structures of cellulose. Fig. 2 shows 2D ^{13}C-^{13}C RFDR and PDSD spectra of the *Brachypodium* cell wall at 800 MHz. A short RFDR mixing time of 1.5 ms was used to detect one-bond cross peaks while a 30 ms PDSD spin diffusion mixing time was used to measure multi-bond cross peaks [8, 16, 20]. Comparison of the two spectra allowed us to assign multiple sets of cellulose chemical shifts. Although the C3 and C5 chemical shifts are similar (around 72 ppm), and both carbons are bonded to C4, the 2D RDFR spectrum yields unambiguous C5 chemical shifts from the C5-C6 cross peaks, thus distinguishing the C5 from the C3 chemical shift. The 2D PDSD spectrum exhibits all intra-residue cross peaks, the most characteristic ones being the C1-C4 and C4-C6 cross peaks. Fig. S2 shows examples of how the 2D RFDR and PDSD spectra are used together to resolve the signals of interior cellulose types *a* and *d*. Starting from the C1-C4 cross peaks in the PDSD spectrum, we can identify the C6-C4 cross peaks in the PDSD spectrum, followed by the C6-C5 and C4-C5 cross peaks in the RFDR spectrum. The C4-C5 cross peaks further correlate to C4-C3 cross peaks in the RFDR spectrum to give the C3 chemical shift. The C4-C5 cross peaks also connect to C4-C1, C4-C6 and other cross peaks in the PDSD spectrum to confirm the other chemical shifts. The starting C1-C4 cross peak in the PDSD spectrum can also be traced to the C1-C2 cross peak in the RFDR spectrum to obtain the C2 chemical shifts. It is noteworthy that a single C1-C2 cross peak at (105, 72.6) ppm is observed for cellulose types *b, d, f*, and *g*, but the narrow C2 linewidth of 1.2 ppm makes the C2 chemical shift assignment unambiguous. This situation differs from the resonance overlap often encountered in disordered proteins, where the broad linewidths lead to multiple possible assignments [54, 55]. Consistent with the literature, the two types of surface cellulose (*f* and *g*) exhibit C4 and C6 chemical shifts that are 3-4 ppm smaller than (i.e. upfield from) the chemical shifts of interior cellulose. Similar 2D PDSD spectra were measured for the other primary cell walls, and the multiple sets of cellulose ^{13}C chemical shifts of *Brachypodium*, *Zea Mays* and *Arabidopsis* are summarized in Table 1.

In total, the high-field 2D correlation spectra resolved five types of interior cellulose (*a*-*e*) and two types of surface cellulose (*f* and *g*), indicating significant structural heterogeneity of plant primary-wall cellulose (Fig. 3, S3). Fig. 3 compares the most important C6-C4 and C1-C4 regions of the five plant cell walls, including three *Arabidopsis* cell walls and two grass cell walls. The three *Arabidopsis* samples include a WT sample, a xyloglucan-deficient mutant, and a CESA mutant with reduced cellulose synthesis capability. As can be seen, the seven types of cellulose are observed in most cell walls but with varying intensities. For example, cellulose *c* signals are strong in *Brachypodium* and *Arabidopsis* cell walls, but much weaker in the *Zea Mays* cell wall. Table 2 lists the estimated percentages of the different cellulose subtypes in the cell walls investigated here. As we show below, cellulose *c* can be assigned to glucan chains that are more than one chain away from the microfibril surface [19], thus its lower intensity in *Zea Mays* suggests that the microfibrils of *Zea Mays*

may have smaller lateral dimensions and fewer core chains. The *Brachypodium* cell wall has negligible amount of cellulose *e*, whose C4 chemical shift of 90 ppm matches that of the Iα crystalline allomorph. Importantly, cellulose *d* is absent in the xyloglucan-deficient *xxt1xxT2xxt5* mutant, suggesting that cellulose *d* is responsible for contacting hemicellulose. The two grass cell walls, which contain negligible xyloglucan but have glucoarabinoxylan (GAX) as the major hemicellulose [17], also show clear cellulose *d* signals (Fig. 3a, b), indicating that GAX interacts with cellulose microfibrils in a similar fashion as xyloglucan in dicot cell walls. The CESA mutant was previously found to reduce the cellulose crystallinity [32]. Consistently, the cellulose peaks of this mutant cell wall are broader and less defined (Fig. 3e).

Differences between primary-wall cellulose and crystalline bacterial, algal and animal cellulose

To gain insight into the structures underlying these chemical shifts, we compared the measured primary-wall cellulose chemical shifts with values reported for highly crystalline cellulose of *Cladophora* and tunicate [7] (Fig. 4). *Cladophora* is rich in Iα cellulose, which is formed by identical chains that each contains two alternating types of glucose units, A and A' [8, 10]. Tunicate cellulose is dominated by the Iβ allomorph, which contains two types of glucose residues (B and B') separated into alternating sheets [8, 9]. We show in Fig. 4 the chemical shift differences between the five primary wall interior cellulose *a-e* and the four types of crystalline Iα and Iβ cellulose. Both the average chemical shift RMSD values and the individual ^{13}C chemical shift differences are shown to indicate the structural similarities and differences between different sources of cellulose. The chemical shifts of most carbons in the structurally known and distinct Iα and Iβ allomorphs (Table 1) differ by less than 1.0 ppm, with the exceptions of C5 of Iα A and A' and C1 of Iα B and B', whose chemical shifts differ by 2.0-2.5 ppm. Thus, we chose a cutoff of 1.5 ppm for an individual carbon as an indication that two structures are significantly different. In general, C1, C4 and C6 chemical shifts are sensitive to the glycosidic ϕ (O5-C1-O1-C4) and ψ (C1-O1-C4-C5) torsion angles and the χ' (C4-C5-C6-O6) torsion angle, which dictates the C6 hydroxymethyl conformation [56].

Fig. 4 and Table 1 show that cellulose *e* matches the Iα allomorph glucose A' very well, with a chemical shift RMSD of only 0.5 ppm. Moreover, no individual ^{13}C chemical shift has large discrepancy with the literature values. Thus, cellulose *e* can be confidently assigned to a conformation and hydrogen-bonding pattern that are similar to the Iα A' structure. However, the other four types of interior cellulose cannot be assigned satisfactorily to any Iα and Iβ structures. For cellulose *a-c*, even the best fits with the crystalline cellulose allomorphs have chemical shift RMSDs of ~1.0 ppm, and individual differences of more than 1.5 ppm are observed for some carbons. For example, cellulose *a* shows best matches with glucose A and B' in the Iα and Iβ allomorphs, respectively, but the C2 chemical shift of cellulose *a* deviates by 1.7 ppm from the A C2 chemical shift, suggesting differences in hydrogen bonding near C2 (e.g. O2-O6), while the C1 chemical shift of cellulose *a* differs by 1.8 ppm from the C1 chemical shift of glucose B' (Table 1). Similarly, cellulose *b* has significantly different C2 and C3 chemical shifts from those of B' and A.

Interestingly, cellulose *d*, which interacts with xyloglucan, exhibits the worst agreement with any known crystalline cellulose structures. The chemical shift RMSDs range from 1.1 to 1.6 ppm (Fig. 4a). Five out of six carbons in cellulose *d* are more than 1.0 ppm different from the chemical shifts of cellulose B, which best matches cellulose *d* (Fig. 4b). This poor agreement is consistent with assignment of cellulose *d* to glucan chains that interact with hemicellulose, which do not exist in crystalline cellulose of non-plant organisms. We previously found that expansin, a wall-loosening protein [21, 57, 58], targeted these limited regions of cellulose microfibrils where xyloglucan was entrapped [59]. The expansin-bound cellulose has a unique C4 chemical shift, 1.0 ppm upfield from the average cellulose C4 signal, and resembles the cellulose *d* C4 chemical shift seen here. Thus, cellulose *d* may play an important role in wall loosening.

These chemical shifts indicate that except for cellulose *e*, whose structure matches that of cellulose A' well, the other four types of interior cellulose in plant primary walls do not resemble the glucose structures in crystalline bacterial and algal cellulose. Fig. 4b shows two best assignments each for cellulose *a* to *c*: *a*-A/B', *b*-B'/A, and *c*-B/B', while cellulose *d* is unique to plant primary cell walls. These results indicate that primary wall cellulose does not have the same structure as bacterial, algal and animal cellulose, and the long-held conceptual framework of Iα and Iβ allomorphs as the basic structural units of native cellulose do not adequately describe plant primary wall cellulose. In addition to chemical shift differences of individual carbons, the intensity distribution is not consistent with the equimolar ratio of A and A' or B and B' (Table S2), which are required for the Iα and Iβ allomorph. For example, while cellulose *e* chemical shifts match the cellulose A' chemical shifts well, neither *a* or *b* cellulose, which have partial resemblance to the A structure, have similar intensities to the cellulose *e* peaks in the spectra. For all the cell walls examined here, spectral intensities indicate that the percentages of cellulose *a* and *b* are the highest among all interior cellulose types, followed by cellulose *c*, while cellulose *d* and *e* are present at low concentrations (Table 2). These results indicate that primary wall celluloses have distinct structures from the Iα and Iβ structures, and matrix polysaccharides have significant influences on the packing and conformation of the glucan chains.

Comparison of plant primary wall cellulose with secondary wall cellulose

Cellulose in secondary cell walls has also been studied extensively using NMR; thus it is interesting to compare its chemical shifts with the primary-wall cellulose results here. In wood, cellulose microfibrils are estimated to be 10 - 20 nm across [60], and their order has been investigated by deconvolution of 1D ^{13}C solid-state NMR spectra [61–63]. The results indicate that pulping changes the cellulose structure, converting some of the Iα structure to the Iβ allomorph. 2D ^{13}C-^{13}C correlation spectra of extracted and regenerated wood cellulose showed a large distribution of chemical shifts [64, 65] and indicated the presence of not only crystalline cellulose Iα and Iβ allomorphs but also cellulose II, which consists of antiparallel packed glucan chains. This cellulose II structure is the result of the regeneration process and thus cannot be extended to native primary-wall cellulose. Recently, Dupree and coworkers used 2D and 3D ^{13}C correlation solid-state NMR experiments to investigate the structure of intact dried *Arabidopsis* secondary walls. They resolved three sets of cellulose chemical shifts [66], two of which match those of interior cellulose types *b* and *c* found here,

while the third set matches the surface cellulose *f* in our samples (Table 1). This suggests that a subset of the cellulose structure and packing may be conserved between the primary and secondary cell walls, and the conserved sub-types are evenly distributed in the core of the microfibril, between the core and the surface, and on the surface. Consistent with our current observations, these authors found no evidence of the Iβ allomorph in the secondary-wall cellulose. Taken together, these data suggest that cellulose in untreated and native plant primary and secondary cell walls share structural similarities, and both differ significantly from the crystalline cellulose found in bacteria, algae and animals.

DFT calculations of cellulose chemical shifts

To gain insight into the structures underlying the multiple sets of cellulose ^{13}C chemical shifts, we carried out DFT calculations of chemical shifts for cellulose with varying hydroxymethyl conformations. Density functional theory has been demonstrated to be a powerful tool for reproducing experimentally measured NMR chemical shifts of crystalline cellulose [38, 39] and for refining the structures of small molecules [67]. We created energy-minimized structural models of Iα and Iβ cellulose [9, 10] with three hydroxymethyl conformations: *tg*, *gt*, *gg* (Table S1, Fig. 5). Following the crystal structure, the Iβ allomorph contains two non-equivalent glucan chains, the origin (O) and center (C) chains, which lie in alternating layers, while Iα cellulose comprises the same glucan chains, each containing alternating non-equivalent glucose residues U and D. To calculate the chemical shifts of the interior U, D, O, C residues, we used minimal numbers of 48 and 28 glucose residues for the Iβ and Iα allomorphs, respectively. Fig. 6 compares the measured and calculated (Table 3) ^{13}C chemical shifts of these glucose residues. All measured interior cellulose (*a*-*e*) chemical shifts agree well with the calculated C6 chemical shifts for the *tg* conformation, with an RMSD of ~2.1 ppm (Table S3), which is close to the best agreement we have achieved when comparing calculated and observed $\delta^{13}C$ values on known structures [38, 39, 68, 69]. In addition, cellulose *d*, which interacts with matrix polysaccharides, shows good agreement with the calculated chemical shifts for the Iβ *gt* conformer (Fig. 6b), suggesting that *tg* and *gt* conformations may coexist in the plant-specific cellulose *d*. None of the measured chemical shifts agree with the calculated values for the *gg* conformation, indicating that the *gg* conformer is energetically unfavorable in interior cellulose.

Spatial distribution and intermolecular contacts of different cellulose in plant primary cell walls

To obtain information about how the different cellulose structures interact with water and matrix polysaccharides and where they are located in the microfibril, we measured water-edited 2D correlation spectra and long-mixing-time 2D correlation spectra. A ^{1}H T_2 filtered PDSD experiment was used to select the water ^{1}H magnetization and transfer it to neighboring polysaccharides [33]. Fig. 3f shows the water-edited spectrum of the *Brachypodium* cell wall. The signals of cellulose *a* and *b* are well retained in the water-edited spectrum whereas the *c* and *d* signals are preferentially suppressed, indicating that cellulose *a* and *b* are close to the microfibril surface while cellulose *c* and *d* are more sequestered from water. The different distribution of cellulose with respect to water is consistent with recently reported ^{1}H-^{13}C 2D correlation spectra, which show much narrower ^{13}C signals for water-proximal cellulose than the full ^{13}C signals of all

cellulose [18, 70, 71]. The current water-edited 2D ^{13}C-^{13}C correlation spectrum shows the retention of the 89-ppm C4 chemical shift, which is the frequency of cellulose *a* and *b*, while the C4 peaks of cellulose *c* and *d* at 87 and 88 ppm have been suppressed.

2D PDSD correlation spectra measured with a long ^{13}C spin diffusion mixing time of 1.0 s (Fig. 7a, Fig. S4) provided valuable information about the spatial contacts between different forms of cellulose. A large number of intermolecular cross peaks between the two types of surface cellulose, between surface and interior cellulose, and between different types of interior cellulose, are observed in the 1.0 s spectrum (Fig. 7b, c). For example, the 61.5 ppm cellulose-*g* C6 cross section shows a clear cross peak with cellulose *f* C6 at 62.5 ppm, indicating *f*-*g* contacts on the microfibril surface. Both *g*C6 and *f*C6 show cross peaks with interior cellulose C6 at 65 ppm. Interestingly, the surface-surface *g*-*f* cross peaks have similar intensities as the surface-interior cross peaks in both the 1.0 s PDSD spectrum and the 0.2 s PDSD spectrum (Fig. S5), strongly suggesting that *g* and *f* glucose rings do not reside in the same chain. The distances between adjacent glucose rings in the same chain are 2-3 Å, while the shortest distance between glucose in two different chains are 4-6 Å. Since spin diffusion rates are inversely proportional to the distance to the sixth power [72], if *f* and *g* are mixed in the same chain, then they would give rise to ~64-fold faster buildup and hence much stronger cross peaks than the surface-interior cross peaks, which is inconsistent with the data. It is also unlikely for *g* and *f* cellulose to be segregated onto different microfibril surfaces such as hydrophobic and hydrophilic surfaces, since this would make the distances too large to observe. Therefore, the 2D spectra indicate that cellulose *g* and *f* are well mixed chains on the same microfibril surface (Fig. 8). Further, these two types of surface chains have similar populations, since their intensities are similar in all spectra.

Multiple cross peaks are detected between surface and interior cellulose, but among interior cellulose *a*-*d*, cellulose *c* C6 has the weakest cross peak with the surface *g*/*f* C6 (Fig. 7b), indicating that cellulose *c* is the furthest away from the microfibril surface. This is consistent with the observation that cellulose *c* is inaccessible to water in the water-edited 2D spectra (Fig. 3f). In addition, the *a*/*b* C4 cross section at 88.9 ppm shows cross peaks with both the surface *g*/*f* C4 and with interior cellulose *c* C4 (Fig. 7c), suggesting that cellulose *a* and *b* are sandwiched between the core cellulose *c* and the surface cellulose. The presence of cross peaks between all significantly populated interior cellulose types (*a*-*d*) is important, as it indicates that the different cellulose structures are not separated into different microfibrils or along the long axis of the microfibril, but rather coexist laterally within each microfibril.

^{13}C T_1-filtered 2D PDSD spectra show that all interior cellulose ^{13}C intensities decayed to ~62% after 4 s, indicating similar ^{13}C T_1 relaxation times of 8.4 s (Fig. S6), while the surface cellulose signals have faster relaxation, to ~ 55%, corresponding to a ^{13}C T_1 of ~6.7 s. The shorter T_1 of surface cellulose indicates faster nanosecond motions than interior cellulose, while the similarity of the *f* and *g* cellulose T_1 relaxation times is consistent with the intimate mixing of these chains. Similarly, the fact that all interior cellulose types have similar ^{13}C T_1 relaxation times indicates that they are tightly packed to each other, which is consistent with the strong cross peaks between different types of interior cellulose in the 1.0 s PDSD spectrum.

Combining the chemical shift information, the water-edited spectra, and the long-mixing-time spectra, we propose the following structural motifs and spatial locations of the various cellulose polymorphs in the plant primary-wall microfibril (Fig. 8). Surface cellulose *f* and *g* are well hydrated but separate chains that are well mixed on the microfibril surface. In the core of the microfibril lies cellulose *c*, with characteristic C1 and C4 chemical shifts of 104 ppm and 88 ppm. This cellulose does not contact the surface chains, does not interact with matrix polysaccharides, and is poorly hydrated. Between cellulose *c* and the surface cellulose lie cellulose conformations *a* and *b*, which are well hydrated and are in direct contact with the surface cellulose. Interior cellulose *e* is found at a low population in all cell walls, but is particularly depleted in grass cell walls. The most interesting cellulose in the primary cell walls is cellulose *d*. Multiple lines of evidence indicate that cellulose *d* is more disordered than other interior cellulose and interacts extensively with other polysaccharides. First, its C4 chemical shift of 87 ppm (Table 1) is smaller than that of other interior cellulose and is the closest to the surface cellulose C4 chemical shift, suggesting that cellulose *d* has structural similarity to the surface cellulose. Second, mutant cell wall spectra indicate that cellulose *d* interacts with hemicellulose in both dicot cell walls (xyloglucan) and grass cell walls (xylan). Third, cellulose *d* exhibits strong cross peaks with surface cellulose (Fig. 7) but is poorly hydrated (Fig. 3f). This paradox can be resolved if cellulose *d*, despite being on the microfibril surface, forms a sufficiently large hydrophobic assembly with hemicellulose that decreases its hydration. This hypothesis is supported by molecular dynamics simulations that suggested that xyloglucan can bind multiple cellulose microfibrils to form a sandwiched cellulose-hemicellulose-cellulose junction that provide mechanical strength to cell walls [73] (Fig. 8) as well as acting as biomechanical “hotspots” [74, 75] for wall loosening by expansin [59]. Alternatively, cellulose *d* may reside inside the microfibril, but some hemicellulose chains may intercalate sufficiently into the microfibrils to restructure some of the glucan chains to form this structure. Fourth, while all interior cellulose types adopt the *tg* conformation for the exocyclic C6, cellulose *d* also has a significant propensity to form the *gt* conformer, which is absent in the Iα and Iβ structures [9, 10] but which has been attributed to exist in surface cellulose [76]. Binding to hemicellulose may be partly responsible for this alternative C6 conformation. Thus, overall, cellulose *d* has mixed structural characteristics of interior cellulose and surface cellulose.

The observed structural polymorphism of primary-wall cellulose is more pronounced than that of crystalline microbial cellulose. While the Iα and Iβ allormorphs with a total of four resolvable sets of chemical shifts are well known for bacterial and algae cellulose, the Iα and Iβ conformations do not coexist in the same microfibril. This is supported by high-resolution synchrotron and neutron diffraction data [9, 10] as well as the lack of Iα to Iβ cross peaks in solid-state NMR spectra of bacterial and tunicate cellulose [8]. The coexistence of as many as seven structures in each microfibril is thus unique to plant cell wall cellulose, and is consistent with the nature of the plant cell wall as a network of different polysaccharides together carrying out the mechanical and growth functions of the wall. In comparison, bacteria and algae secrete pure cellulose, in the absence of other polysaccharides, and the cellulose microfibrils assemble into large and highly water-absorbent sheets on the cell surface [77–79]. The different molecular-level polymorphism of the plant and microbial celluloses thus likely underlie the distinct macroscopic physical and functional properties.

The structural polymorphism of the cellulose chains on the microfibril surface and in the interior indicates a lack of uniformity in the interactions of cellulose with matrix polysaccharides, thus cell wall structural models that depict cellulose as being uniformly coated by a layer of hemicellulose, such as the covalently crosslinked model and the diffuse layer model [58], are unlikely. In comparison, the tethered network model and the stratified layer model both posit xyloglucan to crosslink cellulose microfibrils at specific positions, thus they can in principle be consistent with the observed cellulose chemical shift multiplicity. However, these two models both consider pectins as separate from the cellulose-hemicellulose chains, which is not consistent with the reported intermolecular cross peaks between cellulose and pectins [14–16, 19]. Thus the tethered network model and the stratified layer model must also be modified to include pectins into the cellulose-hemicellulose network. In comparison, recent solid-state NMR data, biochemical assays and atomic force microscopy data suggest that cellulose interacts with xyloglucan only in limited positions but contact pectins extensively [13, 14, 16, 19]. This model is consistent with the structural polymorphism of cellulose in primary cell walls.

Conclusions

The above high-field 2D ^{13}C-^{13}C correlation solid-state NMR spectra of ^{13}C-labeled plant primary cell walls resolved seven cellulose structures, five of which corresponding to interior cellulose. ^{13}C chemical shifts indicate that most of these interior cellulose structures differ significantly from the Iα and Iβ structures found in the crystalline cellulose of bacteria, algae, and animals. DFT calculations indicate that interior cellulose types *a, b* and *c* adopt the *tg* hydroxymethyl conformation, while interior cellulose *d* may adopt a mixture of *tg* and *gt* conformations. Importantly, 2D correlation spectra detailing intermolecular water-polysaccharide and polysaccharide-polysaccharide contacts show that all interior celluloses are well mixed on the sub-nanometer scale. The surface cellulose *f* and *g* are separate chains that are adjacent to each other on the same microfibril surface, interior cellulose *c* is sequestered in the core of the microfibril and is dehydrated, while interior cellulose *a* and *b* are in contact with the surface. The most interesting cellulose, cellulose *d*, is poorly hydrated, interacts with hemicellulose, and is targeted by expansin during wall loosening. Cellulose *d* may either lie on the microfibril surface as part of a hydrophobic assembly with hemicellulose or reside in the microfibril but is disordered by embedded hemicellulose. Together, these results indicate that plant primary wall cellulose is much more polymorphic than microbial cellulose, and this structural difference is likely caused by different biosynthetic and assembly pathways of cellulose in the different organisms, as well as the intimate macromolecular interactions of the primary-wall cellulose with matrix polysaccharides, which do not exist in bacterial or algal cellulose [13].

Supplementary Material

Refer to Web version on PubMed Central for supplementary material.

Acknowledgments

This work is supported by the Center for Lignocellulose Structure and Formation, an Energy Frontier Research Center funded by the U.S. Department of Energy, Office of Science, Basic Energy Sciences under Award # DE-

SC0001090. Portions of this research were conducted with Advanced CyberInfrastructure computational resources provided by the Institute for CyberScience at The Pennsylvania State University (http://ics.psu.edu). The 900 MHz spectra were measured at the MIT/Harvard Center for Magnetic Resonance, which is supported by NIH grant EB002026. The authors thank Prof. Karl Mueller and Brittney Nagle for providing the *Zea Mays* sample.

Abbreviations

Rha, R	rhamnose
Ara, A	arabinose
I	interior crystalline cellulose
s	surface amorphous cellulose
GalA, GA	galacturonic acid
G	glucose in xyloglucan
GAX	glucuronoarabinoxylan
Xyl, x	xylose
solid-state NMR	Solid-State nuclear magnetic resonance
CP	cross polarization
MAS	magic-angle spinning
PDSD	protondriven spin diffusion
RFDR	radio frequency-driven recoupling
INADEQUATE	incredible natural-abundance double-quantum transfer experiment

References

1. Jarvis M. Chemistry: cellulose stacks up. Nature. 2003; 426:611–612. [PubMed: 14668842]
2. Pauly M, Keegstra K. Cell-wall carbohydrates and their modification as a resource for biofuels. The Plant journal : for cell and molecular biology. 2008; 54:559–568. [PubMed: 18476863]
3. Horii F, Hirai A, Kitamaru R. Solid-state high-resolution C-13 NMR studies of regenerated cellulose samples with different crystallites. Polymer Bulletin. 1982; 8:163–170.
4. Atalla RH, Vanderhart DL. Native cellulose: a composite of two distinct crystalline forms. Science. 1984; 223:283–285. [PubMed: 17801599]
5. Vanderhart DL, Atalla RH. Further ^{13}C NMR evidence for the coexistence of two crystalline forms in native celluloses. ACS Symposium Series. 1987; 340:88–118.
6. Kono H, Yunoki S, Shikano T, Fujiwara M, Erata T, Takai M. CP/MAS ^{13}C NMR study of cellulose and cellulose derivatives. 1. Complete assignment of the CP/MAS ^{13}C NMR spectrum of the native cellulose. J. Am. Chem. Soc. 2002; 124:7506–7511. [PubMed: 12071760]
7. Kono H, Erata T, Takai M. Determination of the through-bond carbon-carbon and carbonproton connectivities of the native celluloses in the solid state. Macromolecules. 2003; 36:5131–5138.
8. Kono H, Numata Y. Structural investigation of cellulose I_α and I_β by 2D RFDR NMR spectroscopy: determination of sequence of magnetically inequivalent D-glucose units along cellulose chain. Cellulose. 2006; 13:317–326.

9. Nishiyama Y, Langan P, Chanzy H. Crystal structure and hydrogen-bonding system in cellulose I_β from synchrotron X-ray and neutron fiber diffraction. J. Am. Chem. Soc. 2002; 124:9074–9082. [PubMed: 12149011]
10. Nishiyama Y, Sugiyama J, Chanzy H, Langan P. Crystal structure and hydrogen bonding system in cellulose I_β, from synchrotron X-ray and neutron fiber diffraction. J. Am. Chem. Soc. 2003; 125:14300–14306. [PubMed: 14624578]
11. Carpita NC. Structure and biogenesis of the cell walls of grasses. Annu. Rev. Plant Phys. 1996; 47:445–476.
12. Carpita NC, Gibeaut DM. Structural models of primary cell walls in flowering plants: consistency of molecular structure with the physical properties of the walls during growth. The Plant journal : for cell and molecular biology. 1993; 3:1–30. [PubMed: 8401598]
13. Cosgrove DJ. Re-constructing our models of cellulose and primary cell wall assembly. Curr. Opin. Plant Biol. 2014; 22C:122–131.
14. Dick-Perez M, Zhang YA, Hayes J, Salazar A, Zabotina OA, Hong M. Structure and interactions of plant cell wall polysaccharides by two- and three-dimensional magic-angle-spinning solid-state NMR. Biochemistry-Us. 2011; 50:989–1000.
15. Dick-Perez M, Wang T, Salazar A, Zabotina OA, Hong M. Multidimensional solidstate NMR studies of the structure and dynamics of pectic polysaccharides in uniformly ^{13}C-labeled Arabidopsis primary cell walls. Magn. Reson. Chem. 2012; 50:539–550. [PubMed: 22777793]
16. Wang T, Zabotina O, Hong M. Pectin-cellulose interactions in the *Arabidopsis* primary cell wall from two-dimensional magic-angle-spinning solid-state nuclear magnetic resonance. Biochemistry-Us. 2012; 51:9846–9856.
17. Wang T, Salazar A, Zabotina OA, Hong M. Structure and dynamics of *Brachypodium* primary cell wall polysaccharides from two-dimensional ^{13}C solid-state nuclear magnetic resonance spectroscopy. Biochemistry-Us. 2014; 53:2840–2854.
18. Wang T, Park YB, Cosgrove DJ, Hong M. Cellulose-Pectin Spatial Contacts Are Inherent to Never-Dried Arabidopsis thaliana Primary Cell Walls: Evidence from Solid-State NMR. Plant Physiol. 2015; 168:871. [PubMed: 26036615]
19. Wang T, Hong M. Solid-state NMR investigations of cellulose structure and interactions with matrix polysaccharides in plant primary cell walls. J. Exp. Bot. 2016; 67:503–514. [PubMed: 26355148]
20. Wang T, Williams JK, Schmidt-Rohr K, Hong M. Relaxation-compensated difference spin diffusion NMR for detecting ^{13}C-^{13}C long-range correlations in proteins and polysaccharides. J. Biomol. NMR. 2015; 61:97–107. [PubMed: 25510834]
21. Cosgrove DJ. Growth of the plant cell wall. Nat. Rev. Mol. Cell Biol. 2005; 6:850–861. [PubMed: 16261190]
22. Kimura S, Laosinchai W, Itoh T, Cui X, Linder CR, Brown RMJ. Immunogold labeling of rosette terminal cellulose-synthesizing complexes in the vascular plant vigna angularis. Plant Cell. 1999; 11:2075–2086. [PubMed: 10559435]
23. Newman RH, Davies LM, Harris PJ. Solid-state ^{13}C nuclear magnetic resonance characterization of cellulose in the cell walls of *Arabidopsis thaliana* leaves. Plant Physiol. 1996; 111:475–485. [PubMed: 12226303]
24. Kennedy CJ, Cameron GJ, Sturcova A, Apperley DC, Altaner C, Wess TJ, Jarvis MC. Microfibril diameter in celery collenchyma cellulose: X-ray scattering and NMR evidence. Cellulose. 2007; 14:235–246.
25. Fernandes AN, Thomas LH, Altaner CM, Callow P, Forsyth VT, Apperley DC, Kennedy CJ, Jarvis MC. Nanostructure of cellulose microfibrils in spruce wood. Proc. Natl. Acad. Sci. U.S.A. 2011; 108:E1195–-E1203. [PubMed: 22065760]
26. Newman RH, Hill SJ, Harris PJ. Wide-angle x-ray scattering and solid-state nuclear magnetic resonance data combined to test models for cellulose microfibrils in mung bean cell walls. Plant Physiol. 2013; 163:1558–1567. [PubMed: 24154621]
27. Thomas LH, Forsyth VT, Sturcova A, Kennedy CJ, May RP, Altaner CM, Apperley DC, Wess TJ, Jarvis MC. Structure of cellulose microfibrils in primary cell walls from Collenchyma. Plant Physiol. 2013; 161:465–476. [PubMed: 23175754]

28. Oehme DP, Downton MT, Doblin MS, Wagner J, Gidley MJ, Bacic A. Unique Aspects of the Structure and Dynamics of Elementary Iβ Cellulose Microfibrils Revealed by Computational Simulations. Plant Physiol. 2015; 168:3-U654. [PubMed: 25786828]
29. Hill JL, Hammudi MB, Tien M. The Arabidopsis Cellulose Synthase Complex: A Proposed Hexamer of CESA Trimers in an Equimolar Stoichiometry. Plant Cell. 2014; 26:4834–4842. [PubMed: 25490917]
30. Zhang T, Mahgsoudy-Louyeh S, Tittmann B, Cosgrove DJ. Visualization of the nanoscale pattern of recently-deposited cellulose microfibrils and matrix materials in never-dried primary walls of the onion epidermis. Cellulose. 2014; 21:853–862.
31. Zhang T, Zheng Y, Cosgrove DJ. Spatial Organization of Cellulose Microfibrils and Matrix Polysaccharides in Primary Plant Cell Walls as Imaged by Multi-Channel Atomic Force Microscopy. The Plant journal : for cell and molecular biology. 2015; 85:179–192.
32. Harris DM, Corbin K, Wang T, Gutierrez R, Bertolo AL, Petti C, Smilgies DM, Estevez JM, Bonetta D, Urbanowicz BR, Ehrhardt DW, Somerville CR, Rose JKC, Hong M, DeBolt S. Cellulose microfibril crystallinity is reduced by mutating C-terminal transmembrane region residues $CESA1^{A903V}$ and $CESA3^{T942I}$ of cellulose synthase. Proc. Natl. Acad. Sci. U.S.A. 2012; 109:4098–4103. [PubMed: 22375033]
33. White PB, Wang T, Park YB, Cosgrove DJ, Hong M. Water-polysaccharide interactions in the primary cell wall of *Arabidopsis thaliana* from polarization transfer solid-state NMR. J. Am. Chem. Soc. 2014; 136:10399–10409. [PubMed: 24984197]
34. Bennett AE, Ok JH, Griffin RG, Vega S. Chemical shift correlation spectroscopy in rotating solids: radiofrequency-driven dipolar recoupling and longitudinal exchange. The Journal of chemical physics. 1992; 96:8624–8627.
35. Hong M, Griffin RG. Resonance Assignment for Solid Peptides by Dipolar-Mediated 13C/15N Correlation Solid-State NMR. J. Am. Chem. Soc. 1998; 120:7113–7114.
36. Rienstra CM, Hohwy M, Hong M, Griffin RG. 2D and 3D 15N-13C-13C NMR chemical shift correlation spectroscopy of solids: assignment of MAS spectra of peptides. J. Am. Chem. Soc. 2000; 122:10979–10990.
37. Vanderhart DL. Natural-Abundance ^{13}C-^{13}C Spin Exchange in Rigid Crystalline Organic-Solids. J Magn Reson. 1987; 72:13–47.
38. Kubicki JD, Mohamed MNA, Watts HD. Quantum mechanical modeling of the structures, energetics and spectral properties of I alpha and I beta cellulose. Cellulose. 2013; 20:9–23.
39. Kubicki JD, Watts HD, Zhao Z, Zhong LH. Quantum mechanical calculations on cellulose-water interactions: structures, energetics, vibrational frequencies and NMR chemical shifts for surfaces of I alpha and I beta cellulose. Cellulose. 2014; 21:909–926.
40. Adamo C, Barone V. Exchange functionals with improved long-range behavior and adiabatic connection methods without adjustable parameters: The mPW and mPW1PW models. The Journal of chemical physics. 1998; 108:664–675.
41. Rassolov VA, Ratner MA, Pople JA, Redfern PC, Curtiss LA. 6-31G* basis set for third-row atoms. J. Comput. Chem. 2001; 22:976–984.
42. Wolinski K, Hinton JF, Pulay P. Efficient implementation of the gauge-independent atomic orbital method for NMR chemical shift calculations. J. Am. Chem. Soc. 1990; 112:8251–8260.
43. Schreckenbach G, Ziegler T. Calculation of NMR Shielding Tensors Using Gauge-Including Atomic Orbitals and Modern Density Functional Theory. J. Phys. Chem. 1995; 99:606–611.
44. Cheeseman JR, Trucks GW, Keith TA, Frisch MJ. A comparison of models for calculating nuclear magnetic resonance shielding tensors. The Journal of chemical physics. 1996; 104:5497–5509.
45. Bühl M, Kaupp M, Malkina OL, Malkin VG. The DFT route to NMR chemical shifts. J. Comput. Chem. 1999; 20:91–105.
46. Wiitala KW, Hoye TR, Cramer CJ. Hybrid Density Functional Methods Empirically Optimized for the Computation of ^{13}C and ^{1}H Chemical Shifts in Chloroform Solution. J. Chem. Theory Comput. 2006; 2:1085–1092. [PubMed: 26633067]
47. Lodewyk MW, Siebert MR, Tantillo DJ. Computational Prediction of ^{1}H and ^{13}C Chemical Shifts: A Useful Tool for Natural Product, Mechanistic, and Synthetic Organic Chemistry. Chem. Rev. 2012; 112:1839–1862. [PubMed: 22091891]

48. Frisch, MJ., Trucks, GW., Schlegel, HB., Scuseria, GE., Robb, MA., Cheeseman, JR., Montgomery, JA., Vreven, T., Kudin, KN., Burant, JC. Gaussian 09 Revision B.01. Wallingford, CT: 2009.
49. Sarotti AM, Pellegrinet SC. A Multi-standard Approach for GIAO ^{13}C NMR Calculations. J. Org. Chem. 2009; 74:7254–7260. [PubMed: 19725561]
50. Watts HD, Mohamed MNA, Kubicki JD. Comparison of Multistandard and TMSStandard Calculated NMR Shifts for Coniferyl Alcohol and Application of the Multistandard Method to Lignin Dimers. The journal of physical chemistry. B. 2011; 115:1958–1970. [PubMed: 21319787]
51. Gottlieb HE, Kotlyar V, Nudelman A. NMR Chemical Shifts of Common Laboratory Solvents as Trace Impurities. J. Org. Chem. 1997; 62:7512–7515. [PubMed: 11671879]
52. Newman RH, Hemmingson JA. ^{13}C NMR distinction between categories of molecular order and disorder in cellulose. Cellulose. 1995; 2:95–110.
53. Kono H, Erata T, Takai M. Complete assignment of the CP/MAS ^{13}C NMR spectrum of cellulose III_I. Macromolecules. 2003; 36:3589–3592.
54. Yang Y, Fritzsching KJ, Hong M. Resonance assignment of the NMR spectra of disordered proteins using a multi-objective non-dominated sorting genetic algorithm. J. Biomol. NMR. 2013; 57:281–296. [PubMed: 24132778]
55. Tycko R, Hu KN. A Monte Carlo/simulated annealing algorithm for sequential resonance assignment in solid state NMR of uniformly labeled proteins with magic-angle spinning. J Magn Reson. 2010; 205:304–314. [PubMed: 20547467]
56. Shklyaev OE, Kubicki JD, Watts HD, Crespi VH. Constraints on Iβ cellulose twist from DFT calculations of ^{13}C NMR chemical shifts. Cellulose. 2014; 21:3979–3991.
57. Cosgrove DJ. Loosening of plant cell walls by expansins. Nature. 2000; 407:321–326. [PubMed: 11014181]
58. Cosgrove DJ. Wall structure and wall loosening. A look backwards and forwards. Plant Physiol. 2001; 125:131–134. [PubMed: 11154315]
59. Wang T, Park YB, Caporini MA, Rosay M, Zhong LH, Cosgrove DJ, Hong M. Sensitivity-enhanced solid-state NMR detection of expansin's target in plant cell walls. Proc. Natl. Acad. Sci. U.S.A. 2013; 110:16444–16449. [PubMed: 24065828]
60. Donaldson L. Cellulose microfibril aggregates and their size variation with cell wall type. Wood Sci. Technol. 2007; 41:443–460.
61. Hult EL, Larsson PT, Iversen T. A comparative CP/MAS ^{13}C NMR study of cellulose structure in spruce wood and kraft pulp. Cellulose. 2000; 7:35–55.
62. Hult EL, Larsson PT, Iversen T. Cellulose fibril aggregation - an inherent property of kraft pulps. Polymer. 2001; 42:3309–3314.
63. Wickholm K, Larsson PT, Iversen T. Assignment of non-crystalline forms in cellulose I by CP/MAS ^{13}C NMR spectroscopy. Carbohydr. Res. 1998; 312:123–129.
64. Cadars S, Lesage A, Emsley L. Chemical shift correlations in disordered solids. J. Am. Chem. Soc. 2005; 127:4466–4476. [PubMed: 15783229]
65. Lesage A, Bardet M, Emsley L. Through-bond carbon-carbon connectivities in disordered solids by NMR. J. Am. Chem. Soc. 1999; 121:10987–10993.
66. Dupree R, Simmons TJ, Mortimer JC, Patel D, Iuga D, Brown SP, Dupree P. Probing the Molecular Architecture of Arabidopsis thaliana Secondary Cell Walls Using Two- and Three-Dimensional ^{13}C Solid State Nuclear Magnetic Resonance Spectroscopy. Biochemistry-Us. 2015; 54:2335–2345.
67. Salager E, Stein RS, Pickard CJ, Elena B, Emsley L. Powder NMR crystallography of thymol. Phys Chem Chem Phys. 2009; 11:2610–2621. [PubMed: 19421517]
68. Watts HD, Mohamed MNA, Kubicki JD. A DFT study of vibrational frequencies and ^{13}C NMR chemical shifts of model cellulosic fragments as a function of size. Cellulose. 2014; 21:53–70.
69. Witter R, Sternberg U, Hesse S, Kondo T, Koch FT, Ulrich AS. ^{13}C chemical shift constrained crystal structure refinement of cellulose Iα and its verification by NMR anisotropy experiments. Macromolecules. 2006; 39:6125–6132.

70. Yao XL, Hong M. Dipolar filtered ^{1}H-^{13}C heteronuclear correlation spectroscopy for resonance assignment of proteins. J. Biomol. NMR. 2001; 20:263–274. [PubMed: 11519749]

71. Yao XL, Schmidt-Rohr K, Hong M. Medium- and long-distance ^{1}H-^{13}C heteronuclear correlation NMR in solids. J Magn Reson. 2001; 149:139–143.

72. Dumez JN, Emsley L. A master-equation approach to the description of proton-driven spin diffusion from crystal geometry using simulated zero-quantum lineshapes. Phys Chem Chem Phys. 2011; 13:7363–7370. [PubMed: 21431110]

73. Zhao Z, Crespi VH, Kubicki JD, Cosgrove DJ, Zhong LH. Molecular dynamics simulation study of xyloglucan adsorption on cellulose surfaces: effects of surface hydrophobicity and side-chain variation. Cellulose. 2014; 21:1025–1039.

74. Park YB, Cosgrove DJ. A revised architecture of primary cell walls based on biomechanical changes induced by substrate-specific endoglucanases. Plant Physiol. 2012; 158:1933–1943. [PubMed: 22362871]

75. Park YB, Cosgrove DJ. Changes in cell wall biomechanical properties in the xyloglucandeficient xxt1/xxt2 mutant of arabidopsis. Plant Physiol. 2012; 158:465–475. [PubMed: 22108526]

76. Vietor RJ, Newman RH, Ha MA, Apperley DC, Jarvis MC. Conformational features of crystal-surface cellulose from higher plants. The Plant journal : for cell and molecular biology. 2002; 30:721. [PubMed: 12061903]

77. Czaja WK, Young DJ, Kawecki M, Brown RM. The future prospects of microbial cellulose in biomedical applications. Biomacromolecules. 2007; 8:1–12. [PubMed: 17206781]

78. Ross P, Mayer R, Benziman M. Cellulose biosynthesis and function in bacteria. Microbiol. Rev. 1991; 55:35–58. [PubMed: 2030672]

79. Klemm D, Heublein B, Fink HP, Bohn A. Cellulose: fascinating biopolymer and sustainable raw material. Angew Chem Int Ed Engl. 2005; 44:3358–3393. [PubMed: 15861454]

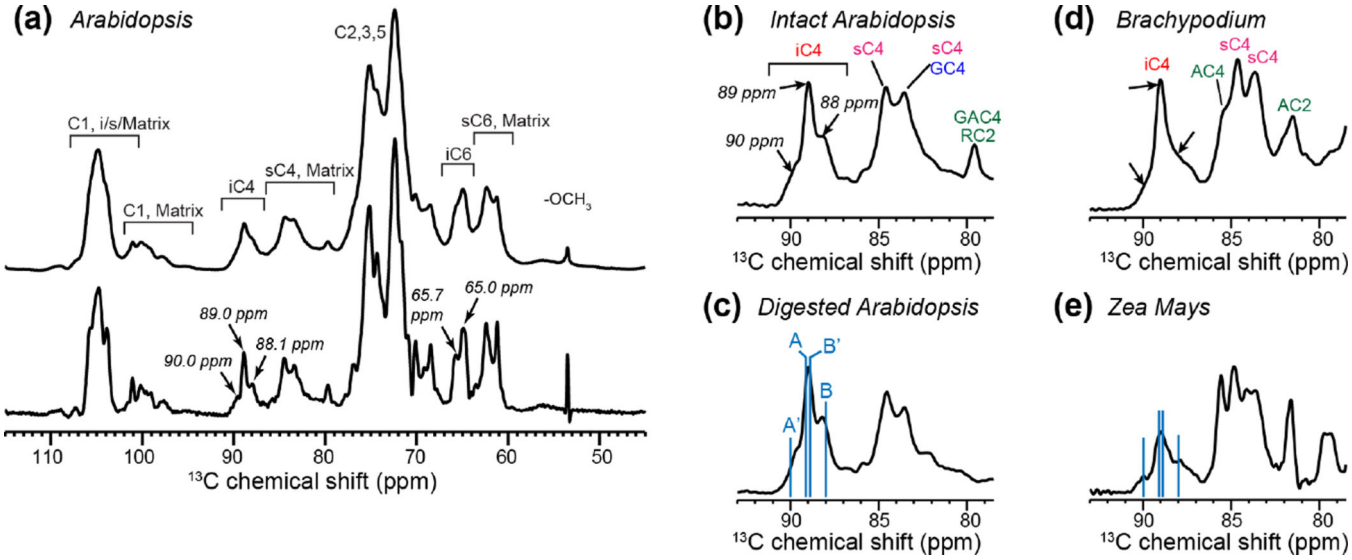

Figure 1.

1D ^{13}C CP-MAS spectra of primary cell walls at high magnetic fields. (a) Never-dried *Arabidopsis* cell walls without (top) and with (bottom) resolution-enhanced window function. The spectrum was measured at 277 K on a 900 MHz spectrometer. The bottom spectrum is processed with a Gaussian function using LB=−140 and GB=0.6. (b-e) C4 region of the ^{13}C spectra of various cell walls. The spectra were measured at 296 K on an 800 MHz NMR, and were processed with LB=−100 and GB=0.6. (b) Intact *Arabidopsis* cell wall. (c) Partially digested *Arabidopsis* cell wall. (d) *Brachypodium* cell wall. (e) *Zea Mays* cell wall. Blue lines in (c) and (e) guide the eye for the literature crystalline cellulose C4 chemical shifts in Iα (A and A') and Iβ (B and B') allomorphs.

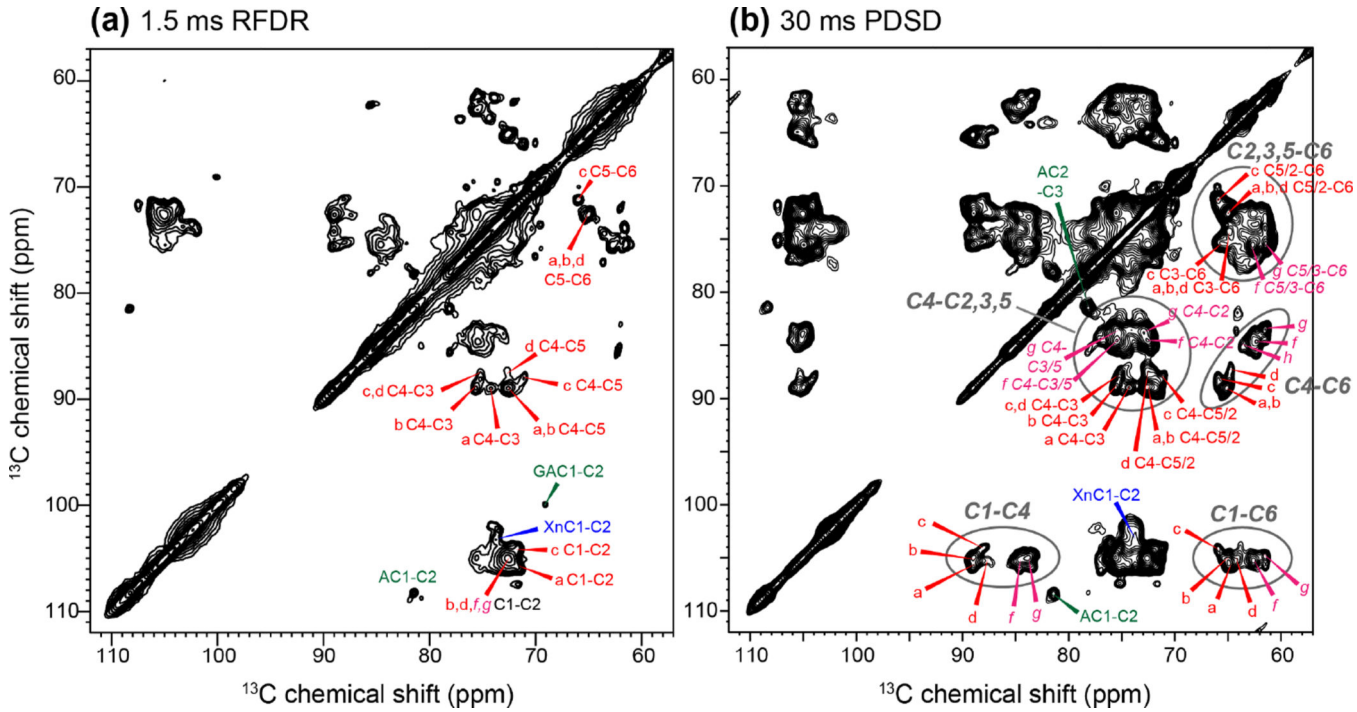

Figure 2.

2D ^{13}C-^{13}C correlation spectra of *Brachypodium* primary cell walls for resonance assignment of the polymorphic cellulose. (a) 1.5 ms RFDR spectrum showing one-bond cross peaks. (b) 30 ms PDSD spectrum showing intra-residue multi-bond cross peaks. The interior and surface cellulose signals are annotated in red and magenta, respectively. Ovals guide the eye for characteristic cross peak regions such as C1-C4, C4-C6 and C1-C6.

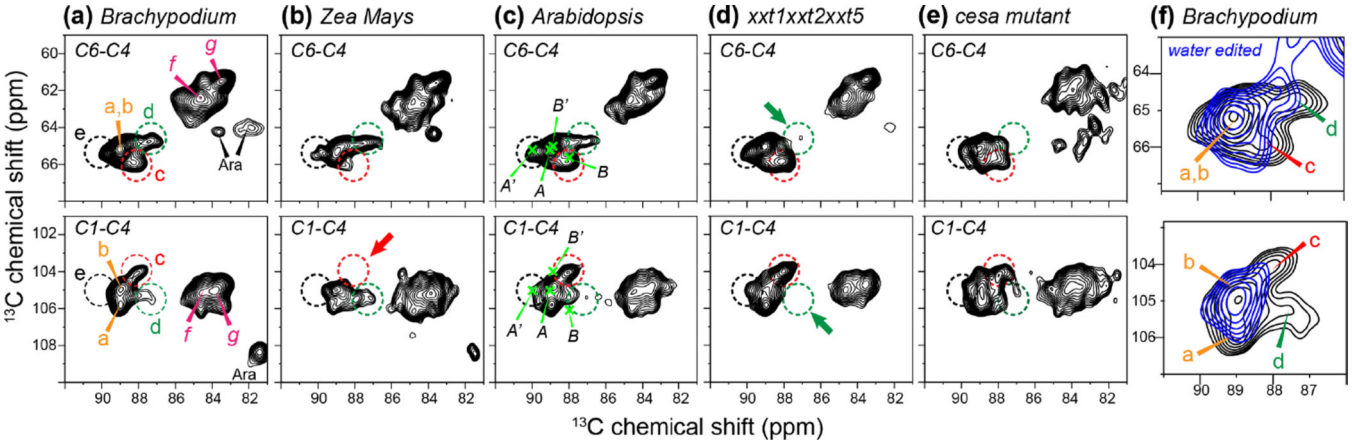

Figure 3.

Comparison of the cellulose C6-C4 (top row) and C1-C4 (bottom row) of the 2D PDSD spectra of various primary cell walls. (a) *Brachypodium* cell wall. (b) *Zea Mays* cell wall. (c) *Arabidopsis* cell wall. (d) *xxt1xxT2xxt5* mutant *Arabidopsis* cell wall. (e) CESA mutant *Arabidopsis* cell wall. Dashed circles guide the eye for the five types of interior cellulose and two types of surface cellulose chemical shifts. (f) Water-edited 2D PDSD spectrum (blue) of the *Brachypodium* cell wall, superimposed with the full PDSD spectrum (black). Cellulose *a* and *b* signals are retained while interior cellulose *c* and *d* signals are suppressed in the water-edited spectrum, indicating the different hydrations of these cellulose structures.

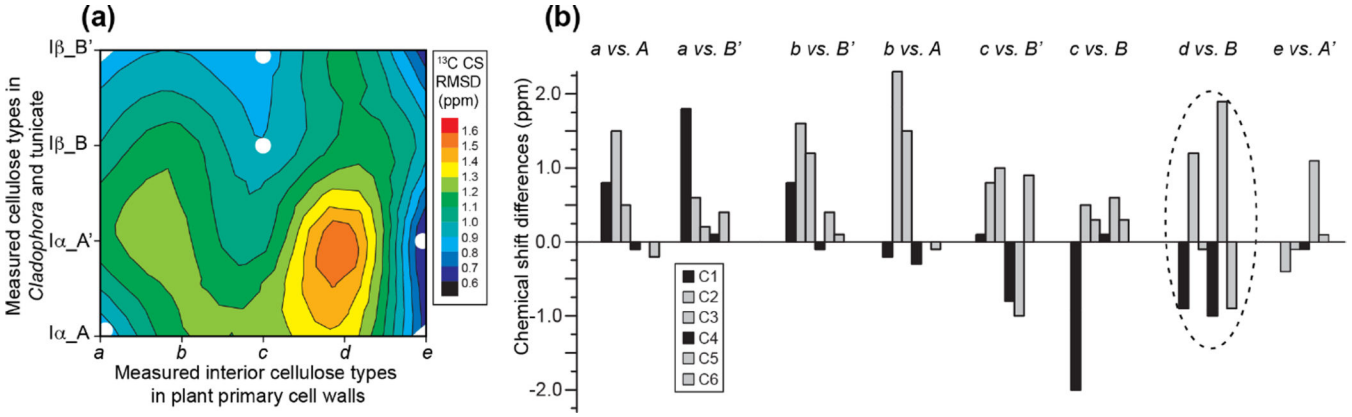

Figure 4.

Comparison of the ^{13}C chemical shifts of plant primary wall cellulose with crystalline cellulose of algae and animals. (a) ^{13}C chemical shift RMSD values between the *Arabidopsis* primary wall interior cellulose *a-e* and literature *Cladophora* and tunicate cellulose, which represent the Iα and Iβ allomorphs, respectively. Each allomorph shows two types of chemical shifts. For ease of inspection, the twenty (5×4) discrete RMSD values are connected by contour lines, thus positions between the twenty points do not have physical meaning. (b) Differences of individual ^{13}C chemical shifts between primary wall celluloses and crystalline Iα and Iβ celluloses. Two similarly good assignments are each found for cellulose *a, b* and *c*, but neither assignment is satisfactory, as shown by chemical shift differences of more than 1.5 ppm for some of the carbons. For cellulose *e*, good agreement with Iα-A' is found. Cellulose *d* has large chemical shift differences from all known allomorphs, indicating that the cellulose *d* structure does not exist in the algal and animal celluloses.

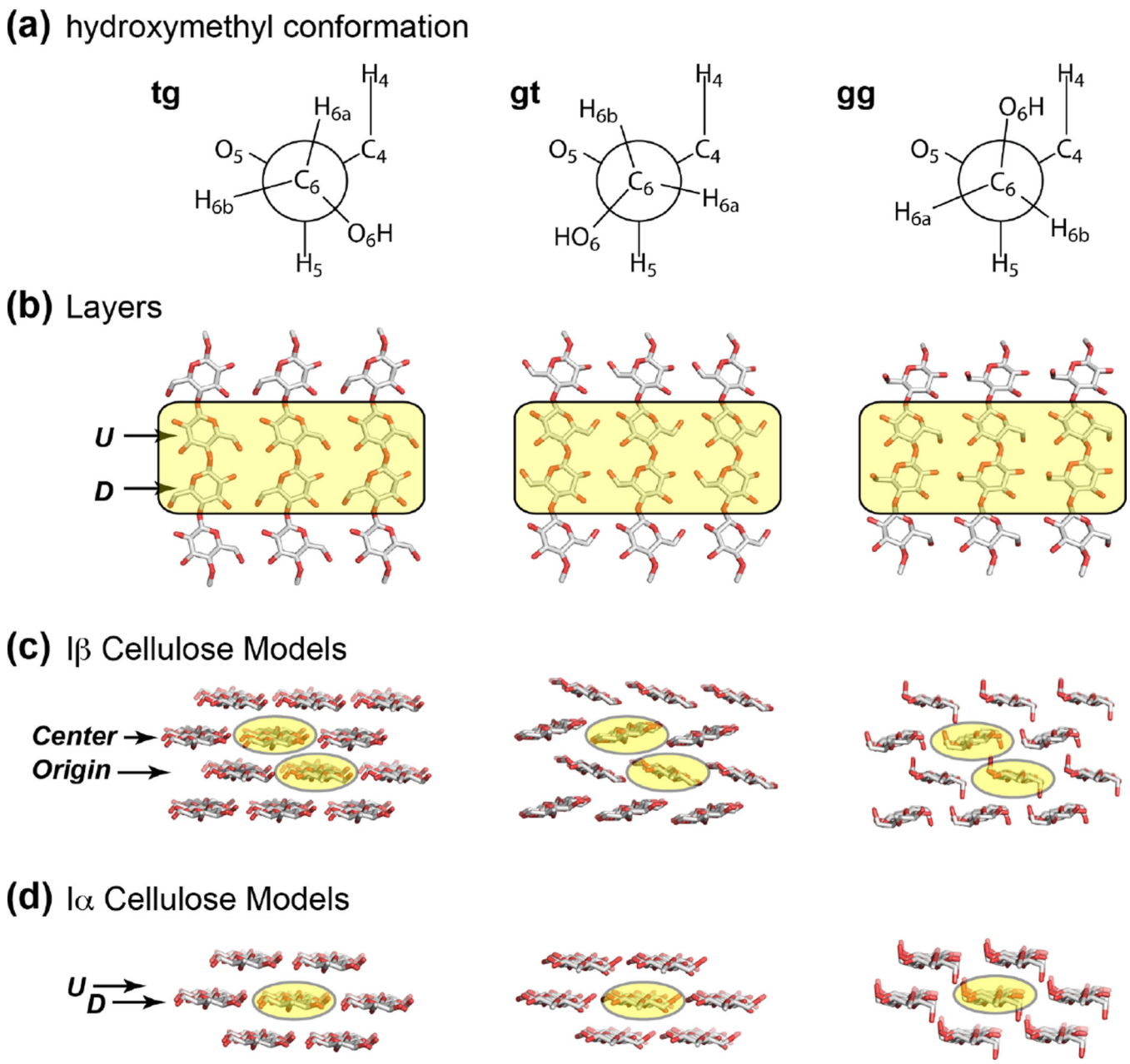

Figure 5.

Cellulose Iα and Iβ structural models with three different C6 conformations: *tg*, *gt* and *gg* from left to right). The shaded glucose residues in each layer were treated as the interior cellulose and were analyzed for ^{13}C and ^{1}H NMR chemical shifts. (a) The three C6 conformations. (b) Face view of a layer of glucan chains in cellulose. U and D denote the two non-equivalent residues in the Iα allomorph. (c) Side view of the Iβ model used to calculate NMR chemical shifts. The center and origin chains are formed by two types of glucose residues in the unit cell of the Iβ crystal structure. (d) Side view of the Iα cellulose structure model. The U and D glucose units alternate along the same chain.

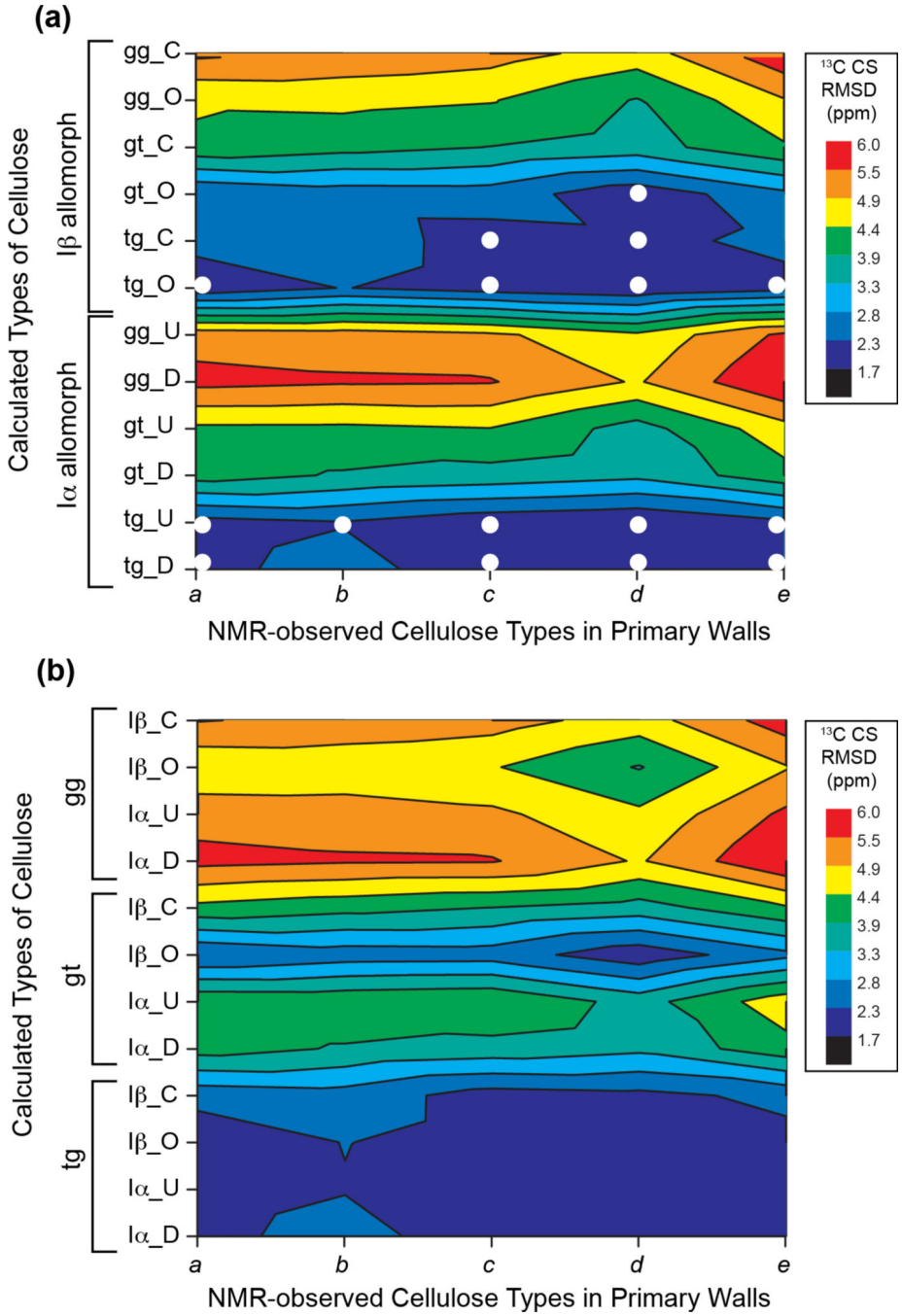

Figure 6.

^{13}C chemical shift RMSDs between measured primary wall cellulose and DFT calculated chemical shifts for various crystalline allomorphs, hydroxymethyl conformations, and glucose residue locations. (a) Calculated cellulose chemical shifts are organized with the Iβ allomorph at the top and the Iα allomorph at the bottom. C and O denote center and origin sheets in the Iβ allomorph [9] while U and D denote the two non-equivalent glucose units in an Iα chain [10]. (b) Calculated cellulose chemical shifts are organized according to the three C6 conformations. *gg* chemical shifts show poor agreement (high RMSD values) with

experimental chemical shifts, while the *tg* conformations show good agreement with measured chemical shifts. The best-matched conformations are indicated as white circles in (a).

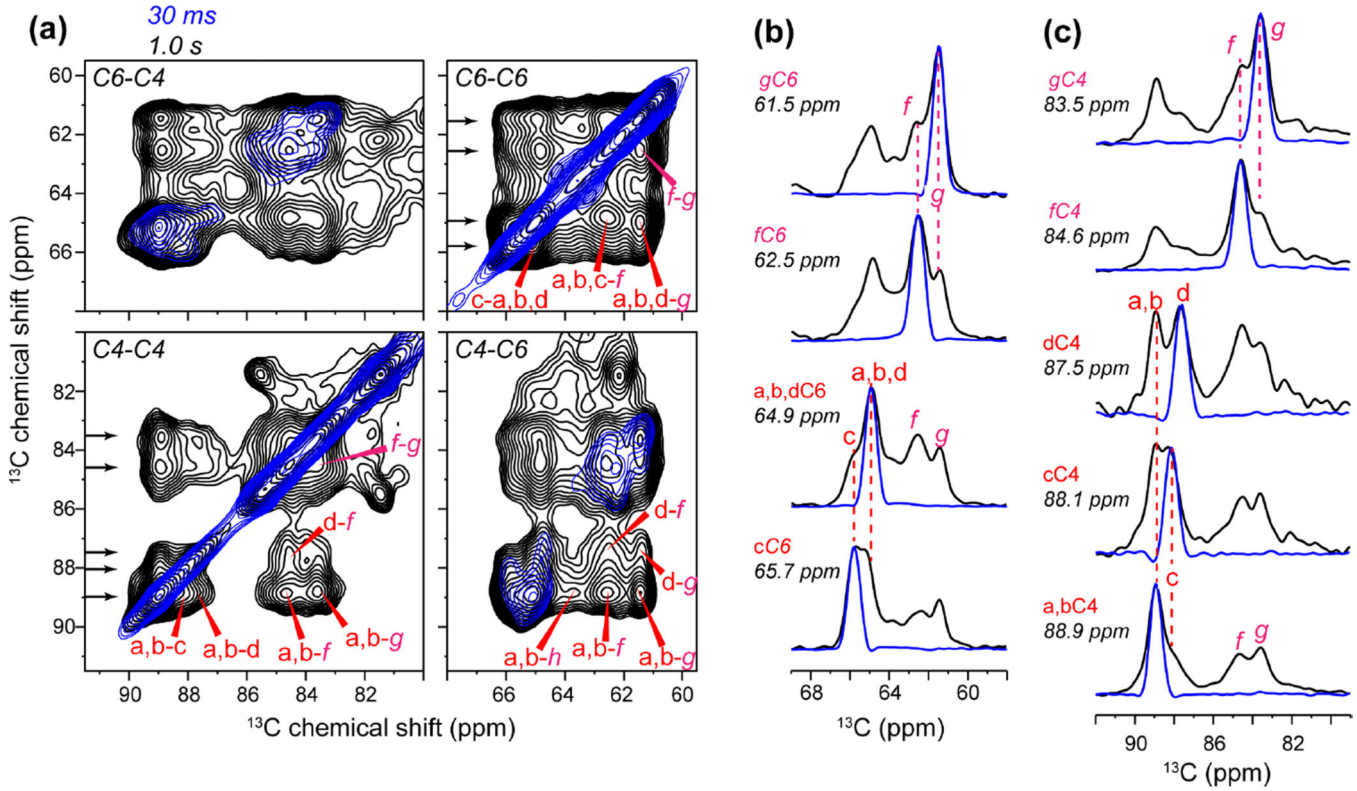

Figure 7.

Intermolecular cross peaks of *Brachypodium* primary wall cellulose from long-mixing-time 2D PDSD spectra. (a) Overlay of the 30 ms PDSD spectrum (blue) and the 1.0 s (black) PDSD spectrum. Long-range cross peaks are assigned. Arrows on the left indicate the extracted 1D cross sections in (b) and (c). (b) Cellulose C6 cross sections. (c) Cellulose C4 cross sections. Interior cellulose *a, b*, and *d* show stronger cross peaks with surface cellulose *f* and *g* compared to interior cellulose *c*.

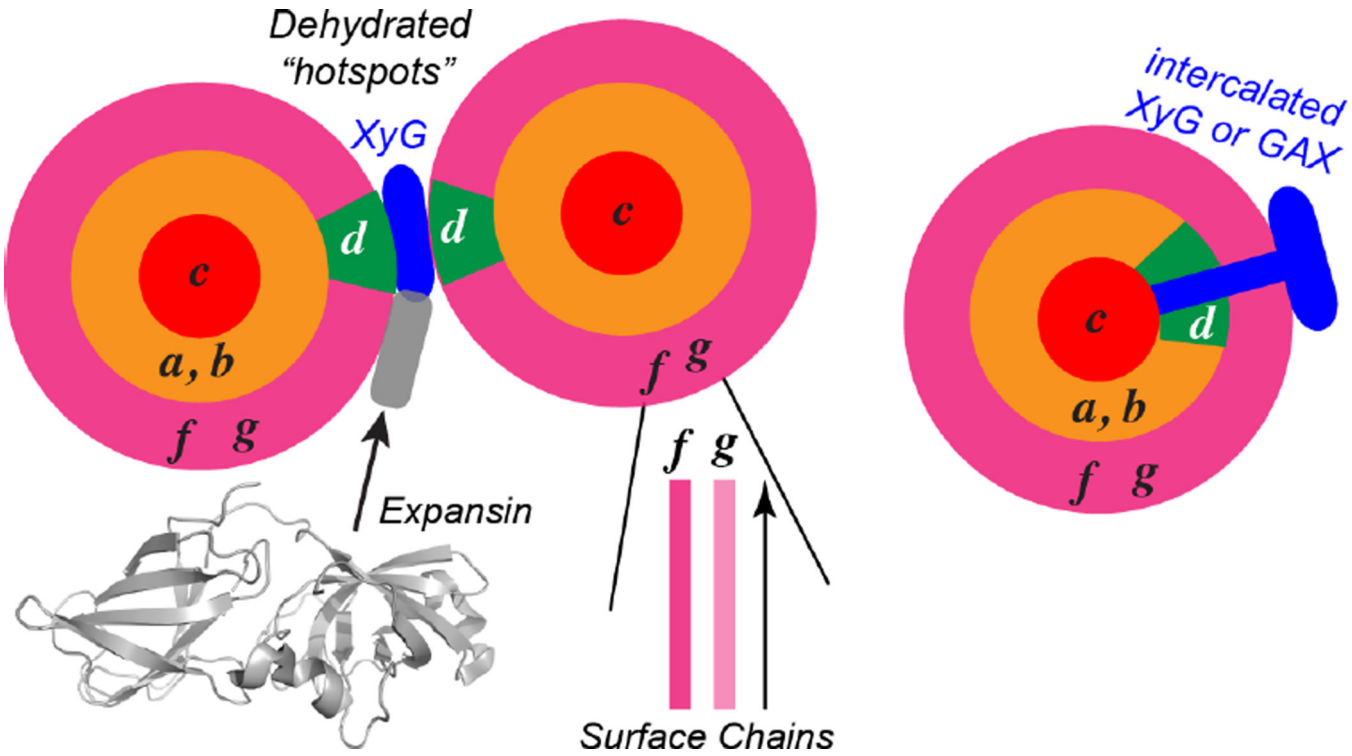

Figure 8.

Proposed model of the spatial distributions and intermolecular contacts of different celluloses in plant primary cell walls. Cellulose *g* and *f* reside on the surface of the microfibril and are well mixed with each other. Cellulose *a* and *b* are interior chains that are associated with the surface chains, while cellulose *c* is embedded in the core of the microfibril, inaccessible to water and not in molecular contact with the surface chains. Cellulose *d* contacts hemicellulose, is targeted by expansins, and is poorly hydrated. Cellulose *d* may lie on the microfibril surface in a hydrophobic assembly with hemicellulose and form part of the biomechanical "hotspots", or may be embedded in the microfibril but disordered due to contact with inserted hemicellulose chains.

Table 1

Cellulose ^{13}C chemical shifts (ppm) of various plant primary cell walls. Weak signals are labeled as (w) and unresolved signals are underlined. *Brachypodium*, *Arabidopsis* and *Zea Mays* primary cell walls are measured in this study. *Cladophora*, tunicate [7, 8] and *Arabidopsis* secondary wall [66] cellulose chemical shifts are literature values.

***Arabidopsis* primary wall cellulose**						
Type	**C1**	**C2**	**C3**	**C4**	**C5**	**C6**
type *a*	105.8	71.6	74.4	89.0	72.6	65.0
type *b*	104.8	72.6	75.4	88.8	72.6	65.5/65.1
type *c*	104.1	71.8	75.2	88.1	71.2	65.9
type *d*	105.2	72.5	74.8	87.0	72.5	64.7
type *e* (w)	105.0	71.2/72.2	74.6	89.9	71.2/72.2	65.3
type *f*	105.1	72.5	75.3/74.1	84.5	75.3	62.5
type *g*	104.9	72.9	75.3	83.5	75.3	61.5
***Brachypodium* primary wall cellulose**						
Type	**C1**	**C2**	**C3**	**C4**	**C5**	**C6**
type *a*	105.8	71.8	74.4	89.1	72.6	64.9
type *b*	105.0	72.6	75.6	89.0	72.6	65.0/65.3
type *c*	104.1	71.8	75.2	88.1	71.1	65.9
type *d*	105.3	72.6	75.2/74.4	87.5/87.0	72.6	64.8/64.1(w)
type *e* (w)	104.8	ND	ND	90.0	ND	65.4
type *f*	105.1	72.9	75.4	84.5	75.4	62.4
type *g*	105.0	72.6	75.3	83.7	75.3	61.6
***Zea Mays* primary wall cellulose**						
Type	**C1**	**C2**	**C3**	**C4**	**C5**	**C6**
type *a*	105.8	71.7	75.7	89.0	72.7	65.0
type *b*	105.0	72.7	75.7/74.0(w)	89.0	72.7	65.3/65.5(w)
type *c*	104.1	71.2	ND	88.0	71.2	66.0
type *d*	105.4	72.8	75.2/75.0/74.5	87.9/87.2	72.6	64.9
type *e* (w)	105.4	72.0	ND	90.1	72.0	65.4

***Arabidopsis* primary wall cellulose**

Type	C1	C2	C3	C4	C5	C6
type *f*	105.2/106.1	72.7	75.7	84.4/84.9	75.7	62.7/63.0
type *g*	105.2	74.2/73.1	74.2/73.1	83.6	75.5	61.6
type *h*	105.4/106.1	73.2	74.7/74.9(w)	85.4	74.7	63.8

***Cladophora* & tunicate cellulose** [7, 8]

Type	C1	C2	C3	C4	C5	C6
Iα A	105.0	70.1	73.9	89.1	72.6	65.2
Iα A’	105.0	71.6	74.7	90.0	70.1	65.2
Iβ B	106.1	71.3	74.9	88.0	70.6	65.6
Iβ B’	104.0	71.0	74.2	88.9	72.2	65.0

***Arabidopsis* secondary-wall cellulose** [66]

Type	C1	C2	C3	C4	C5	C6
Domain 1	105.2	72.4	74.5	88.9	72.7	65.0
	104.1	72.1	74.8	88.1	71.3	65.7
Domain 2	105.2	72.4	74.5	84.2	75.5	62.7

Table 2

Estimated percentages of different cellulose types in plant primary cell walls, obtained by integrating the intensities of C1-C4 cross peaks in the 30 ms PDSD spectra.

Cell walls	*a*	*b*	*c*	*d*	*e*	*f*	*g*
WT *Arabidopsis*	14%	13%	10%	6.0%	3.2%	30%	23%
xxt1xxt2xxt5 Arabidopsis	20%	15%	14%	3.5%	2.9%	24%	21%
Brachypodium	14%	14%	7.6%	6.9%	1.7%	26%	31%
Zea Mays	9.2%	11%	3.3%	8.2%	2.0%	31%	36%

Table 3

DFT calculated cellulose ^{13}C chemical shifts (ppm). U and D denote the two non-equivalent glucose units in the same Iα chain while C and O denote center and origin chains in the Iβ allomorph.

Form	Location	$\delta^{13}C1$	$\delta^{13}C2$	$\delta^{13}C3$	$\delta^{13}C4$	$\delta^{13}C5$	$\delta^{13}C6$
Iα *gg*	U	102.3	70.8	72.8	77.8	72.3	60.0
	D	101.2	73.9	70.8	78.4	74.0	59.0
Iα *gt*	U	103.9	72.1	73.0	81.3	74.0	58.4
	D	98.5	72.6	73.6	83.5	72.5	61.1
Iα *tg*	U	103.6	70.1	72.3	85.7	71.4	63.9
	D	104.2	68.7	72.4	87.3	69.7	64.3
Iβ *gg*	center (C)	100.8	72.9	72.7	77.9	71.6	59.8
	origin (O)	102.9	71.3	70.8	79.8	73.8	61.3
Iβ *gt*	center (C)	99.0	73.4	72.0	83.3	71.1	60.7
	origin (O)	105.2	70.9	71.9	85.2	72.6	62.0
Iβ *tg*	center (C)	103.0	69.7	72.6	85.2	70.1	64.4
	Origin (O)	105.1	69.6	71.8	86.1	71.6	64.3

Biomacromolecules. Author manuscript; available in PMC 2017 January 27.